High-spin state spectroscopy of ^{143}Dy

J. R. B. Oliveira, E. W. Cybulska, N. H. Medina, M. N. Rao, R. V. Ribas, and W. A. Seale
Instituto de Física, Universidade de São Paulo, São Paulo, SP, Brazil

F. R. Espinoza-Quiñones
Departamento de Engenharia Química, Universidade Estadual do Oeste do Paraná (UNIOESTE), Toledo, PR, Brazil

M. A. Rizzutto
Departamento de Ciências Exatas e Tecnológicas, Faculdades Integradas de Guarulhos, Guarulhos, SP, Brazil

D. Bazzacco, F. Brandolini, S. Lunardi, C. M. Petrache, Zs. Podolyák, C. Rossi-Alvarez, and C. A. Ur
Dipartimento di Fisica dell'Università, and INFN, Sezione di Padova, Padova, Italy

G. de Angelis, D. R. Napoli, P. Spolaore, A. Gadea, D. De Acuña, M. De Poli, E. Farnea, D. Foltescu, M. Ionescu-Bujor,* and A. Iordachescu*
INFN, Laboratori Nazionali di Legnaro, Legnaro, Italy
(Received 31 May 2000; published 25 October 2000)

The ^{143}Dy nucleus has been studied with the ^{92}Mo (^{54}Fe, $2pn\gamma$) reaction at 240 MeV incident energy. A rich variety of structures was observed at high spin. The nearly spherical $\nu h_{11/2}$ $I=11/2$ isomer is the basis of a negative parity irregular yrast structure which is observed up to $I=51/2$. A positive parity band presenting a large dynamic moment of inertia was observed, similar to the deformation enhanced $\nu i_{13/2}$ bands known to exist in this mass region. However, we propose an alternative assignment for this band, namely the triaxial collective minimum with $\beta=0.2$ predicted by total Routhian surface calculations for a $N_{\rm osc}=4$ quasineutron excitation coupled to pairs of aligned quasiparticles. Another negative parity structure, with strong $M1$ and weak $E2$ crossover transitions, was observed.

PACS number(s): 21.10.Re, 23.20.En, 23.20.Lv, 27.60.+j

I. INTRODUCTION

Neutron-deficient nuclei in the $A\approx140$ mass region display a rich variety of band structures. Axially symmetric prolate shapes ($\gamma=0°$) are favored for the $h_{11/2}$ quasiproton excitations from the lower midshell in these nuclei with γ-soft cores. The quasineutrons, on the other hand, from the upper part of this shell exert a driving force towards collectively rotating oblate nuclear shapes ($\gamma=-60°$, according to the Lund convention [1]), resulting in shape changes in these nuclei. The systematics of the strongly deformation driving intruder orbital $\nu i_{13/2}$ $[660]1/2^+$ have been extensively investigated in recent years in several odd-N ($N=73,77$) nuclei in the mass 130–140 region (Refs. [2–10]). In ^{133}Nd a g-factor measurement [11] for a positive parity band has confirmed the $\nu i_{13/2}$ configuration assignment. The experimental data obtained up to now in several of these nuclei, including in particular, the measured quadrupole moments, are consistent with the prediction [12] of a quadrupole deformation of $\beta\approx0.35$ for the $\nu i_{13/2}$ configuration, a value close to a prolate nuclear shape with a 3:2 axis ratio. The decoupled $\nu i_{13/2}$ bandhead energies and deformations of odd-N nuclei of this region ($Z=56$–64) and ($N=69$–77) have also been systematically investigated using the Nilsson-Strutinsky method [13].

With a view to extend the systematics of the $i_{13/2}$ band, we recently performed an experiment to produce and investigate extremely neutron deficient Dy nuclei in the $A\approx140$ region, by means of the ^{54}Fe+^{92}Mo reaction at 240-MeV incident energy. Of the various nuclei (with $Z=63$ to 66; $N=75$ to 78) produced in this experiment, the $3p$ channel leading to ^{143}Tb was the strongest one populated at the incident energy used, and the results on the high-spin structures populated in ^{143}Tb were described in [14]. We report here the results on the $2pn$ channel leading to the odd nucleus ^{143}Dy which was among the six most intense channels populated in the experiment. No data on excited states of ^{143}Dy have been published previous to this work.

II. EXPERIMENTAL PROCEDURES

The high spin states in the odd-N nucleus ^{143}Dy have been populated by the ^{92}Mo (^{54}Fe,$2pn\gamma$)^{143}Dy reaction at 240-MeV incident beam energy. The target used was an approximately 1.0 mg/cm^2 thick enriched (>97%) ^{92}Mo foil. The beam was provided by the tandem XTU accelerator of Legnaro National Laboratories. Gamma rays have been detected using the GASP array [15] composed of 40 Compton-suppressed high-efficiency HPGe and the 80-element BGO inner ball. The multi-telescope light-charged-particle detector array (ISIS) [16], consisting of 40 Si surface-barrier $\Delta E-E$ telescopes, enabled the selection of the multiplicities of the evaporated charged particles in coincidence with the observed γ rays. In order to permit the identification of the

*Permanent address: Institute of Physics and Nuclear Engineering, Bucharest, Romania.

 ©2000 The American Physical Society

various masses produced in the reaction, the recoil mass spectrometer (RMS) [17] was coupled to GASP. The coupled GASP-RMS system has an intrinsic mass resolution better than 1/300 and the average transmission efficiency in this experiment was about 1% (efficiencies of this order of magnitude are usual for charged particle emission reactions and with relatively thick targets [18]). Events have been collected on tape when at least two Compton-suppressed HPGe detectors and two BGO detectors fired in coincidence. A total of 1.3×10^9 Compton-suppressed events was collected. The data have been sorted into charged particle-γ-γ, mass-γ-γ and γ-γ-γ cubes.

According to CASCADE code [19] calculations the following cross sections were expected for the evaporation reaction channels: about 100 mb for ^{143}Tb, 40 to 60 mb for each of ^{142}Gd, ^{143}Dy, ^{140}Gd, ^{142}Tb, 20 to 30 mb for each of ^{141}Tb and ^{144}Dy, about 10 mb for each of ^{137,139}Eu, ^{140}Tb and 2 mb or less for ^{141}Dy and others. These predictions are roughly consistent with our experimentally observed yields.

Due to the fact that the efficiency of the charged particle detection system is not 100%, the observed γ-ray spectra gated by charged particle type and fold contain transitions from higher particle multiplicity channels. We have used linear combinations of particle-gated γ-γ matrices to generate clean spectra consisting of transitions from each individual charged particle multiplicity channel of the reaction. As neutrons were not detected, this procedure does not allow the separation of the contribution of different neutron multiplicity channels. The comparison with the mass-143 gated spectra then permitted unambiguous assignment of several γ-transitions to the ^{143}Dy nucleus (Fig. 1). Background-subtracted spectra generated from those matrices were used to construct the level scheme of ^{143}Dy. The data were analyzed using the VAXPAK [20] and RADWARE [21] spectrum analysis codes. The fully symmetrized γ-γ-γ cube was used to construct γ-γ matrices in coincidence with several transitions in each observed cascade. This procedure is particularly important for the weaker transitions (relative intensity below about 3%), which can be confirmed only in the double-gated spectra.

The assignment of the spins and parities to the ^{143}Dy levels was based on the DCO (directional correlation from oriented states) ratios. A γ-γ matrix was constructed by sorting the data from the eight detectors positioned at the 72° and 108° rings in the GASP array against the 12 detectors in the 34° and the 146° rings. Gates were set on both axes on several strong quadrupole transitions and the intensity of other transitions observed in the two spectra has been extracted. If $I_\gamma(72°+108°)$ and $I_\gamma(34°+146°)$ represent the intensity of a transition when gating on the (72°+108°) rings and (34°+146°) rings, respectively, the theoretical DCO ratios

$$R_{\mathrm{DCO}}=\frac{I_\gamma(72°+108°)}{I_\gamma(34°+146°)},$$

which one obtains, for the present geometry, are $R_{\mathrm{DCO}}=1.00$ for quadrupole transitions and $R_{\mathrm{DCO}}=0.55$ for pure dipole transitions. Furthermore, $\Delta I=0$ dipole transitions yield $R_{\mathrm{DCO}}=1.07$.

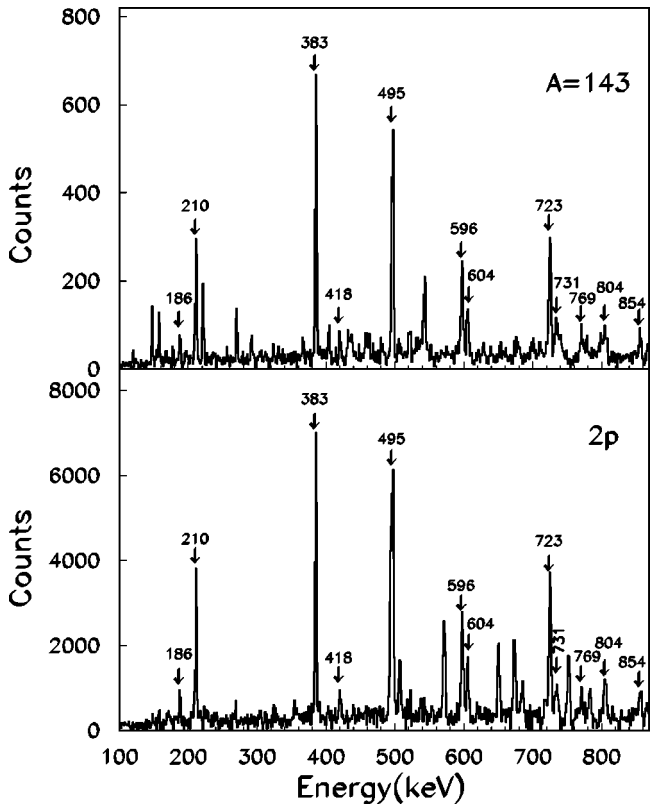

FIG. 1. Gamma-ray spectrum (not efficiency corrected) in coincidence with the 530 keV line (^{143}Dy). (a) Gated with mass 143; (b) gated with particle fold $2p$. The peaks present in both spectra can be assigned to ^{143}Dy. Their energy is shown in keV. The other peaks are contaminants from ^{143}Tb in spectrum (a) and ^{144}Dy in spectrum (b).

III. RESULTS

The level scheme of ^{143}Dy deduced from the present work is shown in Fig. 2. It is consistent with the coincidence relationships, intensity and energy balances from the $2p$-gated matrix and double-gates of the γ-γ-γ cube (except for the cases explicitly mentioned below). The γ-ray energies and relative intensities of all the transitions assigned to ^{143}Dy are given in Table I, which also shows the DCO ratios and the resulting spin and parity assignments. These assignments are, however, all based on the assumption that the spin (parity) of the level populated by the 495 keV transition is $\frac{11}{2}^-$, which is inferred from systematics of the mass region and from the close similarity to the level scheme of the isotone ^{141}Gd [10]. The assignments without parentheses are, therefore, to be regarded as certain, from the DCO results, relative to the spin of that state.

Due to the fact that the $\Delta I=0$ dipole transitions yield an R_{DCO} ratio close to that of a stretched quadrupole, there is an ambiguity of interpretation for the weak transitions (with larger uncertainties). This is the case of the 514 keV transi-

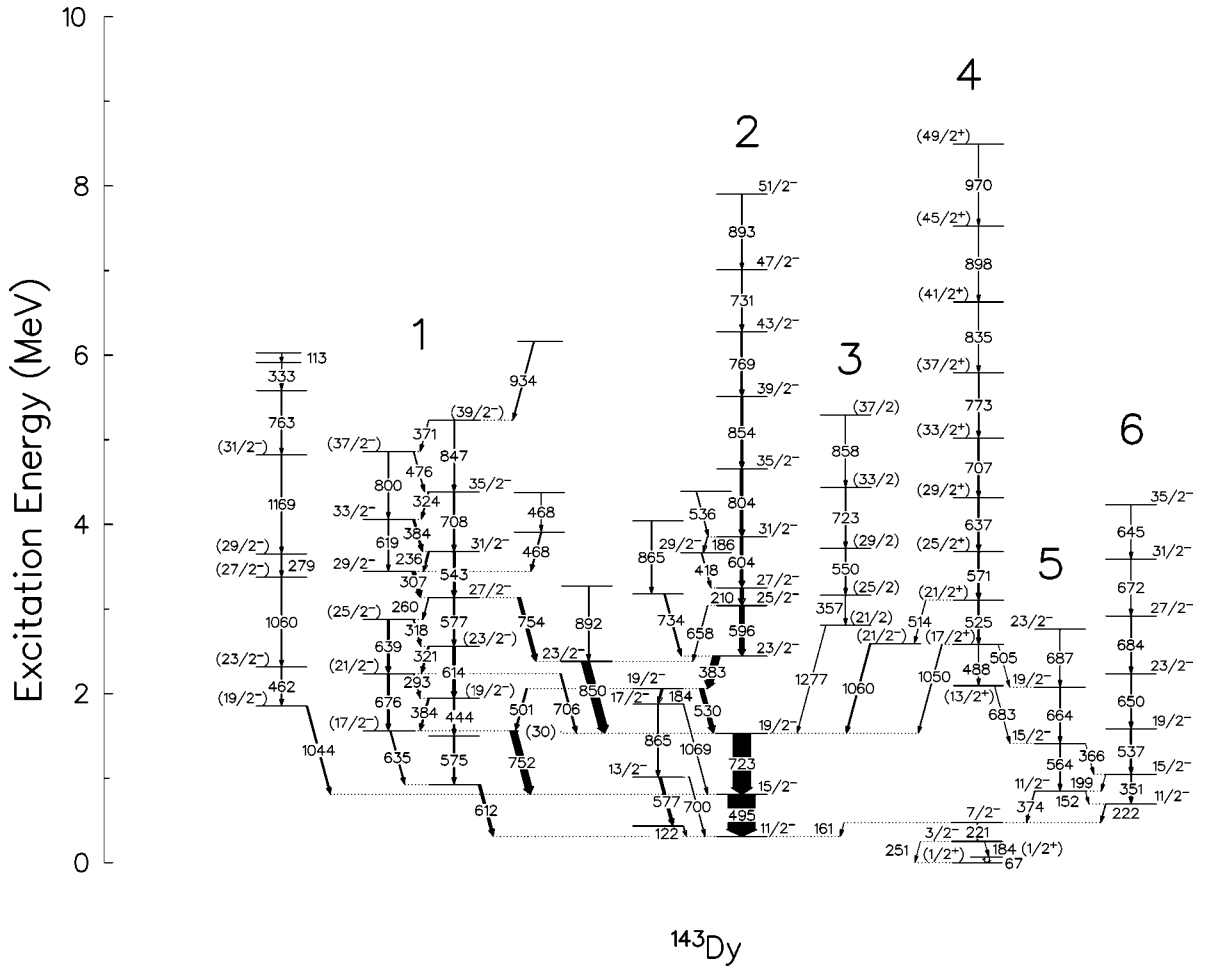

FIG. 2. The level scheme of ^{143}Dy. The energies of the γ-ray transitions are given in keV. The width of the arrows is proportional to the γ -ray relative intensity.

tion linking (together with the 1060 keV line) band 4 to the $\frac{19}{2}^-$ state. For this reason, another possible assignment would be two units larger for all the states of band 4. This ambiguity has no important consequence with regards to the interpretation of this band, discussed below.

There are some alternatives with respect to the ordering of the transitions in the weakly populated cascade presented to the left of structure 1 in Fig. 2. They are presented in order of decreasing relative intensity but other possibilities are consistent within the experimental errors.

Figure 3 shows a sum of clean double gates of the positive parity band of ^{143}Dy (band 4). The coincidence relationships can be verified to be consistent with the observed spectrum. It is apparent from the figure that the sum of the relative intensities of the 184 and 251 keV transitions which decay from the $(\frac{3}{2}^-)$ is significantly below that of the feeding transition 221 keV, indicating that the $(\frac{3}{2}^-)$ state is isomeric and/or its decay is fragmented in additional unobserved lines. A similar situation happens with the lower states of bands 5 and 6. The intensity balance of the $\frac{11}{2}^-$ states shows a loss of observed intensity in the decays. The order of the transitions is fixed, however, by the interband transitions which are well established from the analysis of the double-gated spectra.

IV. DISCUSSION

A. The negative parity bands

The nearly spherical $\nu h_{11/2}$ $I=11/2$ state is the basis of a negative parity irregular yrast structure which is observed in ^{143}Dy (band 2) up to $I=51/2$. The irregularity and the presence of dipole transitions within the cascade indicate a weakly deformed structure. The transitions of structure 2 and the linking transitions between structures 2 and 1 in ^{143}Dy have an almost one-to-one correspondence in ^{141}Gd [10], indicating a strong similarity between the negative parity states. Similar states have been successfully described within the IBFM+ broken pairs model [22] in ^{137}Nd [8] and ^{139}Sm [9]. A stretched $E2$ cascade, band 6 appears to be yrast between spin $I=23/2$ and $I=35/2$. However, it is much less intense than the main sequence (band 2), indicating that it is not fed from higher spin yrast states. There is no clear correspondence between band 6 and the negative parity structures in the neighboring isotones.

Another negative parity band (structure 1, above $I=\frac{27}{2}$), with strong $M1$ and rather weak $E2$ crossover transitions is a possible magnetic rotation band [23,24], based on the $[h_{11/2}]^2$ proton particle pair and $[h_{11/2}]^{-1}$ neutron hole configuration. This type of band appears as a solution of the

TABLE I. Gamma-ray energy, initial and final excitation energy, spin assignments, relative intensity and DCO ratio for the transitions in ^{143}Dy. E_i and E_f are the energies of the initial and final states corresponding to each transition. The γ-ray energies are accurate to ± 0.2 keV rising to ± 0.5 keV for the weak transitions and above 1 MeV. The relative intensities were obtained from the analysis of the $2p$-gated background subtracted (clean) matrix. The uncertainties given may be underestimated for the very weak transitions (below about 3).

E_γ [keV]	E_i [keV]	E_f [keV]	$I_i^\pi \rightarrow I_f^\pi$	I_γ	DCO ratio
(29.9)[a]	1558.0	1529.1	$(17/2^-) \rightarrow 19/2^-$	0.19(3)	
66.7	66.7	0.0	$(1/2^+) \rightarrow (1/2^+)$	2(1)	
112.7	6029.0	5916.2		0.32(3)	0.44(15)
122.1	432.7	310.6	$\rightarrow 11/2^-$	1.0(3)[b]	0.57(15)
151.5	845.3	693.5	$11/2^- \rightarrow 11/2^-$	0.02(3)	
161.2	471.8	310.6	$7/2^- \rightarrow 11/2^-$	0.36(8)	1.08(23)
183.8	2058.7	1874.9	$19/2^- \rightarrow 17/2^-$	4.97(28)	0.52(7)
184.2	250.9	66.7	$3/2^- \rightarrow (1/2^+)$	0.4(5)	1.18(15)
185.7	3851.9	3666.3	$31/2^- \rightarrow 29/2^-$	1.85(11)	
198.7	1044.2	845.3	$15/2^- \rightarrow 11/2^-$	0.07(6)	
209.8	3248.2	3038.4	$27/2^- \rightarrow 25/2^-$	11.11(43)	0.55(6)
220.9	471.8	250.9	$7/2^- \rightarrow 3/2^-$	1.09(21)	1.3(2)
221.8	693.5	471.8	$11/2^- \rightarrow 7/2^-$	1.84(17)	0.94(20)
236.0	3676.2	3440.3	$31/2^- \rightarrow 29/2^-$	5.41(22)	0.61(5)
250.9	250.9	0.0	$3/2^- \rightarrow (1/2^+)$	0.4(4)	1.08(15)
260.0	3133.3	2873.4	$27/2^- \rightarrow (25/2^-)$	2.01(13)	0.60(13)
279.0	3651.0	3372.0	$(29/2^-) \rightarrow (27/2^-)$	2.01(16)	0.59(10)
293.3	2234.7	1941.6	$(21/2^-) \rightarrow (19/2^-)$	2.39(19)	
307.0	3440.3	3133.3	$29/2^- \rightarrow 27/2^-$	12.3(5)	0.57(3)
318.0	2873.4	2555.7	$(25/2^-) \rightarrow (23/2^-)$	3.42(24)	
321.2	2555.7	2234.7	$(23/2^-) \rightarrow (21/2^-)$	5.29(36)	0.58(21)
324.2	4384.2	4060.0	$35/2^- \rightarrow 33/2^-$	3.67(19)	0.45(18)
327.7[c]	3201.1	2873.4	$\rightarrow 25/2^-$	2.4(24)	
333.2	5916.2	5583.1		1.02(10)	0.44(15)
350.7	1044.2	693.5	$15/2^- \rightarrow 11/2^-$	3.65(20)	
356.7	3162.7	2806.0	$(25/2^-) \rightarrow (21/2^-)$	2.1(6)	0.84(7)
366.2	1409.4	1044.2	$15/2^- \rightarrow 15/2^-$	0.14(8)	
370.9	5230.9	4859.9	$(39/2^-) \rightarrow (37/2^-)$	1.52(16)	
373.6	845.3	471.8	$11/2^- \rightarrow 7/2^-$	2.08(23)	0.94(16)
383.5	2442.2	2058.7	$23/2^- \rightarrow 19/2^-$	26.8(12)	0.97(12)
383.8	1941.6	1558.0	$(19/2^-) \rightarrow (17/2^-)$	5.7(6)	
383.9	4060.0	3676.2	$33/2^- \rightarrow 31/2^-$	7.1(5)	
418.4	3666.3	3248.2	$29/2^- \rightarrow 27/2^-$	3.05(25)	0.66(9)
444.4	1941.6	1497.3	$19/2^- \rightarrow$	3.73(29)	
462.3	2312.0	1849.7	$(23/2^-) \rightarrow (19/2^-)$	3.3(5)	1.19(13)
467.6	4376.0	3908.4		0.74(26)	
468.2	3908.4	3440.3	$\rightarrow 29/2^-$	3.9(4)	
475.6	4859.9	4384.2	$(37/2^-) \rightarrow 35/2^-$	2.51(21)	
487.5	2579.1	2091.6	$(17/2^+) \rightarrow (13/2^+)$	1.08(18)	
495.0	805.6	310.6	$15/2^- \rightarrow 11/2^-$	100.0(10)[d]	1.00(6)
501.1	2058.7	1558.0	$19/2^- \rightarrow (17/2^-)$	5.6(5)	
504.5	2579.1	2073.3	$(17/2^-) \rightarrow 19/2^-$	0.21(14)	
513.6	3104.0	2590.0	$(21/2^+) \rightarrow (21/2^-)$	0.88(21)	1.18(33)
524.9	3104.0	2579.1	$(21/2^+) \rightarrow (17/2^+)$	4.2(5)	1.06(17)
529.5	2058.7	1529.1	$19/2^- \rightarrow 19/2^-$	15.8(9)	1.17(7)
535.9	4387.8	3851.9	$\rightarrow 31/2^-$	2.19(29)	
537.3	1581.5	1044.2	$19/2^- \rightarrow 15/2^-$	4.09(27)	1.12(11)

TABLE I. (*Continued*).

E_γ [keV]	E_i [keV]	E_f [keV]	$I_i^\pi \rightarrow I_f^\pi$	I_γ	DCO ratio
542.8	3676.2	3133.3	$31/2^- \rightarrow 27/2^-$	7.7(4)	1.19(15)
550.5	3713.2	3162.7	$(29/2) \rightarrow (25/2)$	2.0(4)	
557.2[c]	4465.6[c]	3908.4		1.49(15)	
564.1	1409.4	845.3	$15/2^- \rightarrow 11/2^-$	3.20(28)	1.04(12)
571.3	3675.2	3104.0	$(25/2^+) \rightarrow (21/2^+)$	6.4(6)	1.25(20)
574.5	1497.3	922.8		5.3(7)	
577.2	1009.9	432.7	$13/2^- \rightarrow$	9.8(14)	0.57(11)
577.4	3133.3	2555.7	$27/2^- \rightarrow (23/2^-)$	5.57(39)	
596.3	3038.4	2442.2	$25/2^- \rightarrow 23/2^-$	17.1(7)	0.46(6)
603.7	3851.9	3248.2	$31/2^- \rightarrow 27/2^-$	10.1(4)	0.92(10)
612.4	922.8	310.6		9.55(10)	
613.9	2555.7	1941.6	$(23/2^-) \rightarrow (19/2^-)$	8.5(6)	
619.2	4060.0	3440.3	$33/2^- \rightarrow 29/2^-$	2.26(23)	
628.2[c]	3666.3	3038.4	$29/2^- \rightarrow 25/2^-$	1.61(29)	
635.3	1558.0	922.8	$(17/2^-) \rightarrow$	4.4(5)	
637.2	4312.4	3675.2	$(29/2^+) \rightarrow (25/2^+)$	5.4(5)	
638.7	2873.4	2234.7	$(25/2^-) \rightarrow (21/2^-)$	8.4(6)	
644.6	4232.1	3587.5	$35/2^- \rightarrow 31/2^-$	0.68(18)	1.1(4)
645.4[c]	3201.1[c]	2555.7	$(27/2^-) \rightarrow (23/2^-)$	5.6(5)	
650.1	2231.6	1581.5	$23/2^- \rightarrow 19/2^-$	4.01(34)	1.25(12)
658.0	3038.4	2379.3	$25/2^- \rightarrow 23/2^-$	1.90(22)	
663.9	2073.3	1409.4	$19/2^- \rightarrow 15/2^-$	2.60(34)	0.95(13)
671.9	3587.5	2915.6	$31/2^- \rightarrow 27/2^-$	1.9(4)	1.33(16)
676.4	2234.7	1558.0	$(21/2^-) \rightarrow (17/2^-)$	6.4(7)	
682.8	2091.6	1409.4	$(13/2^+) \rightarrow 15/2^-$	0.9(4)	
684.0	2915.6	2231.6	$27/2^- \rightarrow 23/2^-$	2.89(24)	1.2(2)
686.9	2760.2	2073.3	$23/2^- \rightarrow 19/2^-$	1.24(25)	
700.2	1009.9	310.6	$13/2^- \rightarrow 11/2^-$	1.9(6)	
706.2	2234.7	1529.1	$(21/2^-) \rightarrow 19/2^-$	5.4(6)	
707.3	5019.7	4312.4	$33/2^- \rightarrow 29/2^-$	5.0(4)	
707.9	4384.2	3676.2	$35/2^- \rightarrow 31/2^-$	5.4(4)	1.15(13)
722.7	4435.9	3713.2	$(33/2) \rightarrow (29/2)$	1.3(4)	
723.4	1529.1	805.6	$19/2^- \rightarrow 15/2^-$	68.4(29)	1.08(4)
731.4	7010.3	6279.0	$47/2^- \rightarrow 43/2^-$	4.54(25)	1.1(2)
733.6	3175.7	2442.2	$\rightarrow 23/2^-$	5.1(6)	
752.5	1558.0	805.6	$(17/2^-) \rightarrow 15/2^-$	25.8(22)	
753.8	3133.3	2379.3	$27/2^- \rightarrow 23/2^-$	12.2(8)	1.05(7)
762.6	5583.1	4820.4	$\rightarrow (31/2^-)$	1.92(29)	
769.4	6279.0	5509.5	$43/2^- \rightarrow 39/2^-$	6.06(31)	1.01(18)
773.5	5793.2	5019.7	$(37/2^+) \rightarrow (33/2^+)$	3.14(37)	
799.8	4859.9	4060.0	$(37/2^-) \rightarrow 33/2^-$	2.39(34)	
803.6	4655.6	3851.9	$35/2^- \rightarrow 31/2^-$	10.6(5)	1.12(13)
821.7[c]	3201.1[c]	2379.3	$\rightarrow 23/2^-$	3.9(6)	
835.4	6628.6	5793.2	$(41/2^+) \rightarrow (37/2^+)$	2.09(28)	
847.1	5230.9	4384.2	$(39/2^-) \rightarrow 35/2^-$	3.41(35)	
850.0	2379.3	1529.1	$23/2^- \rightarrow 19/2^-$	30.5(16)	1.08(3)
854.0	5509.5	4655.6	$39/2^- \rightarrow 35/2^-$	7.35(38)	1.12(17)
858.4	5294.3	4435.9	$(37/2) \rightarrow (33/2)$	1.00(21)	
864.6	4040.3	3175.7		2.6(4)	
865.0	1874.9	1009.9	$17/2^- \rightarrow 13/2^-$	4.1(7)	1.26(7)[e]
892.4	3271.6	2379.3	$\rightarrow 23/2^-$	3.7(6)	
893.1	7903.5	7010.3	$51/2^- \rightarrow 47/2^-$	1.84(18)	1.16(28)

TABLE I. (*Continued*).

E_γ [keV]	E_i [keV]	E_f [keV]	$I_i^\pi \rightarrow I_f^\pi$	I_γ	DCO ratio
898.5	7527.1	6628.6	$(45/2^+) \rightarrow (41/2^+)$	0.81(25)	
934.2	6165.1	5230.9	$\rightarrow 39/2^-$	3.48(30)	
970.4	8497.4	7527.1	$(49/2^+) \rightarrow (45/2^+)$	0.24(22)	
1044.1	1849.7	805.6	$(19/2^-) \rightarrow 15/2^-$	5.4(19)	1.09(16)
1049.9	2579.1	1529.1	$(17/2^+) \rightarrow 19/2^-$	2.3(5)	0.68(24)
1060.1	3372.0	2312.0	$(27/2^-) \rightarrow (23/2^-)$	2.9(5)	0.61(9)
1060.1	2590.0	1529.1	$(21/2^-) \rightarrow 19/2^-$	4.8(12)	0.35(16)
1069.4	1874.9	805.6	$17/2^- \rightarrow 15/2^-$	1.66(36)	
1169.5	4820.4	3651.0	$(31/2^-) \rightarrow (29/2^-)$	1.86(23)	0.55(16)
1276.9	2806.0	1529.1	$(21/2) \rightarrow 19/2^-$	1.5(6)	0.57(10)

[a]Gamma-ray below experimental energy threshold. Inferred indirectly from coincidence relations.
[b]Observed intensity. Probable decay from isomeric state leading to underestimated value.
[c]Tentative gamma ray or level. Not shown in level scheme for simplicity.
[d]Sum of the intensities of the transitions feeding the $15/2^-$ level: 1044, 752, 1069, and 723 keV, normalized to 100.
[e]Contaminated.

tilted axis cranking model applied to nearly spherical nuclei. The particle and hole excitations tend to couple their angular momenta perpendicularly. In order to generate higher spins the angular momentum vectors of particles and holes gradually align, resembling the closing of a pair of blades. For this reason this type of band is also known as a ''shears band.'' In ^{143}Dy, the $M1$ band appears as a rather irregular band, which is an exception among the neighboring isotones, and may not be the expected band based on the shears mechanism.

The $B(M1)/B(E2)$ ratios obtained for the levels of structure 1 are shown in Fig. 4. The levels below $I=\frac{29}{2}$ present lower values for this ratio than the ones above, suggesting a change in configuration. The $E_\gamma=754$ keV $E2$ interband transition was not considered in the calculation of the ratio for the $I=\frac{27}{2}$ state. In ^{141}Gd [10] there are no $M1$ transitions, observed below spin $\frac{25}{2}$, which connect the $M1$ structure to the $(\frac{17}{2}^-)$ state, as in band 1. The $B(M1)/B(E2)$ ratios for band 1 are relatively small (by a factor of 2–3) as compared to those for the magnetic rotation bands of ^{137}Nd [8] and ^{139}Sm [24].

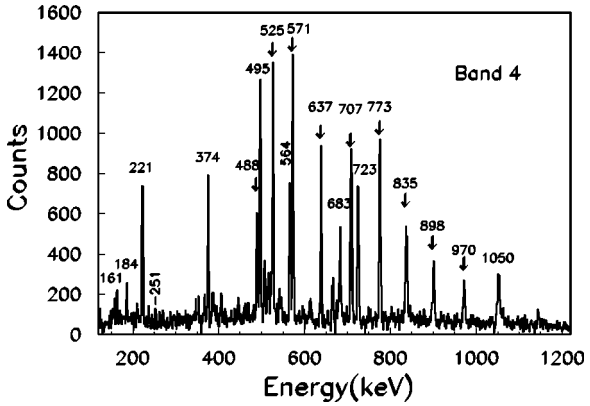

FIG. 3. Sum of clean double gates for the positive parity band of ^{143}Dy (band 4). The in-band transitions are indicated with arrows. The linking transitions, as well as the low lying transitions fed by the band can also be seen.

B. The positive parity band

A very regular structure consisting of stretched $E2$ transitions, presenting a large dynamic moment of inertia, was observed in ^{143}Dy (band 4). It is very tempting to assign to this structure the $\nu i_{13/2}$ configuration, which is known to generate enhanced deformation bands in this region, in particular, in the $N=77$ isotones: ^{137}Nd [8], ^{139}Sm [9], and ^{141}Gd [10]. However the TRS calculations which will be presented in the next subsection indicate another possible interpretation for ^{143}Dy which cannot be ruled out with the presently available experimental data. Figure 5 shows the dynamic moments of inertia for the positive parity bands of the $N=77$ isotones. Both ^{143}Dy and ^{137}Nd show very stable moments of inertia around $60\hbar^2$/MeV. The ^{137}Nd nucleus is the heaviest Nd isotope for which the transition quadrupole moment

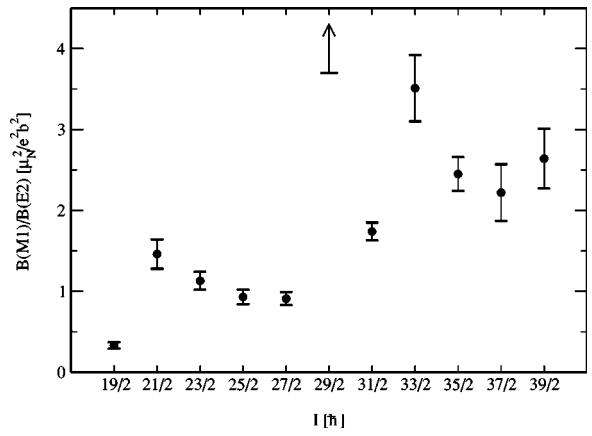

FIG. 4. Ratio of reduced transition probabilities $B(M1)/B(E2)$ as a function of spin for structure 1 in ^{143}Dy.

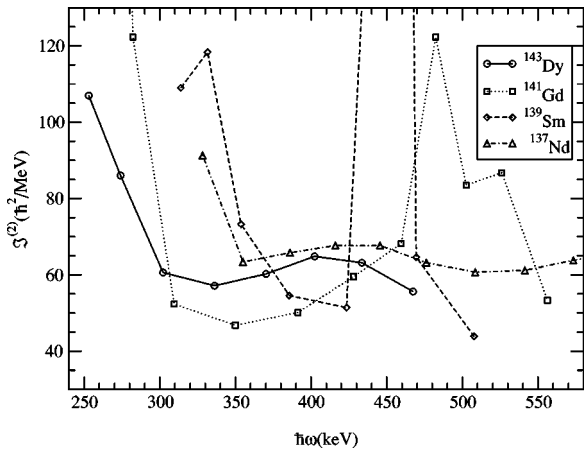

FIG. 5. Dynamic moments of inertia for positive parity bands in $N=77$ isotones (circles ^{143}Dy, squares ^{141}Gd, diamonds ^{139}Sm, and triangles ^{137}Nd).

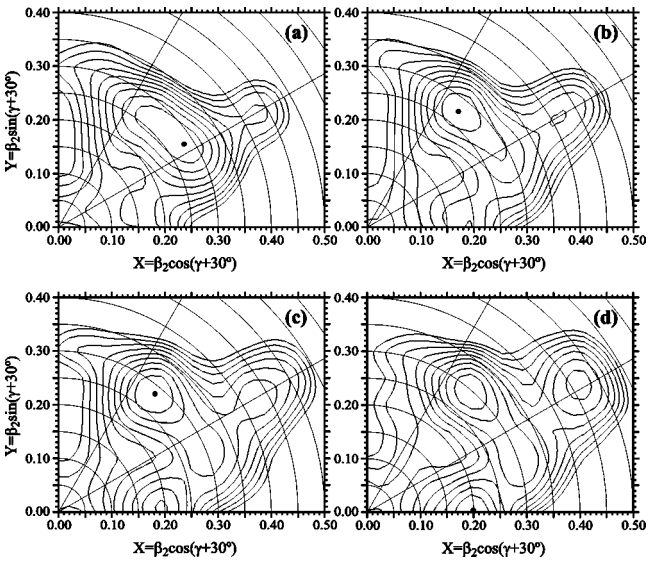

FIG. 6. Total Routhian surface calculations for positive parity configurations at $\hbar\omega\approx 0.5$ MeV in $N=77$ odd nuclei from $Z=60$ to $Z=66$: (a) ^{137}Nd, (b) ^{139}Sm, (c) ^{141}Gd, and (d) ^{143}Dy.

of the $\nu i_{13/2}$ band has been measured. It has the least deformed $i_{13/2}$ band of the Nd isotopes since the number of neutrons is departing from the $N=72$ gap, whose role in stabilizing enhanced deformations has been discussed in an article by Kondev *et al.* [25].

C. Theoretical calculations

Standard total Routhian surface (TRS) calculations [12] were obtained for the yrast positive parity configurations in the $N=77$ isotones. The results, presented in Fig. 6, show an interesting trend as one increases the number of protons from $Z=60$ to $Z=66$. Besides the $\beta\approx 0.3$ minimum, with positive γ, which has been assigned to the Nd $i_{13/2}$ band, an additional minimum appears around $\beta\approx 0.2$, $\gamma\approx -30°$, which becomes favored in ^{143}Dy. The configuration of this minimum is based on positive parity neutron states of the $N_{\mathrm{osc}}=4$ oscillator shell (from mixed $\nu d_{3/2}, s_{1/2}, g_{7/2}$ states on a spherical basis, or $[400]\frac{1}{2}^+$, $[402]\frac{3}{2}^+$, $[404]\frac{5}{2}^+$, $[402]\frac{5}{2}^+$ and others on the deformed basis) coupled to a broken pair of intruder $N_{\mathrm{osc}}=5$ ($h_{11/2}$) aligned protons. Also, the least excited $N_{\mathrm{osc}}=5$ (from mixed $g_{9/2}, f_{7/2}$ states) neutron pair gradually aligns in the frequency range of the band. This minimum constitutes another possible interpretation for the positive parity band of ^{143}Dy. It should be noted that due to a compensation between the degree of collectivity and deformation, the two minima should present rather similar moments of inertia.

The quasiparticle Routhians for a deformed Woods-Saxon potential calculated for ^{143}Dy are shown in Fig. 7. The deformation and the pairing gap parameters used were obtained from the TRS results (above) at a rotational frequency of

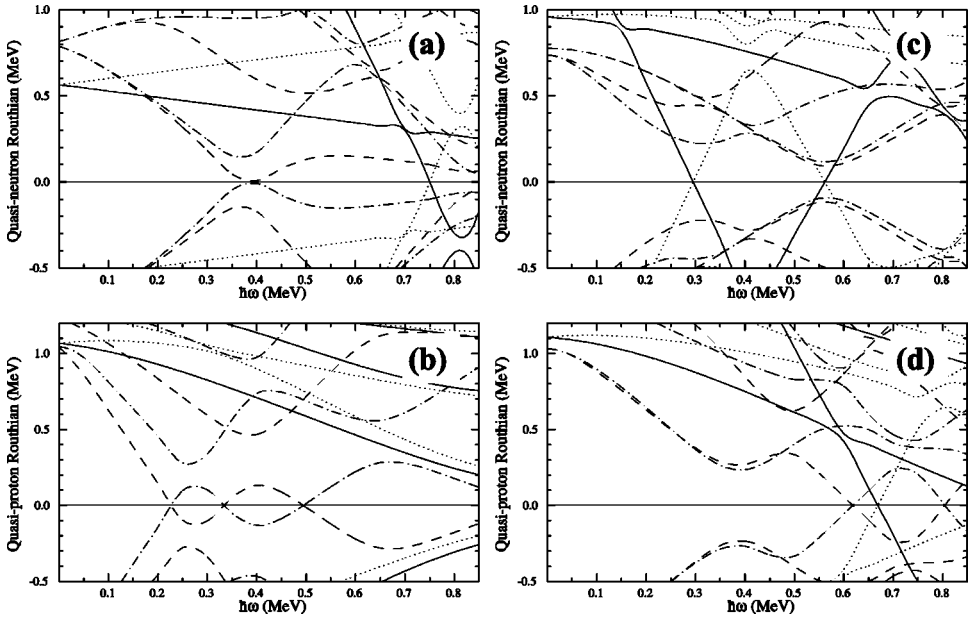

FIG. 7. Quasiparticle Routhians for ^{143}Dy (a) quasineutrons and (b) quasiprotons with deformation parameters corresponding to the absolute minimum of Fig. 3(d): $\beta=0.2$, $\gamma=-30°$; (c) quasineutrons and (d) quasiprotons with deformation parameters corresponding to the $\nu i_{13/2}$ local minimum: $\beta=0.29$, $\gamma=19°$. The line type indicates the parity and signature (π,α): solid $(+,1/2)$, dotted $(+,-1/2)$, dashed $(-,-1/2)$, and dot-dashed $(-,1/2)$.

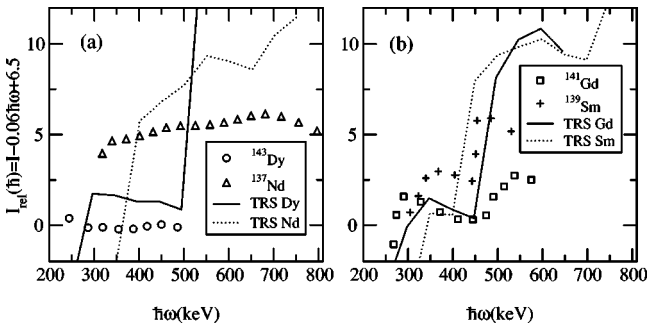

FIG. 8. Relative alignments for the positive parity bands of $N=77$ isotones. A reference of $I_{\mathrm{ref}}=0.06\hbar\omega-6.5$ was subtracted. The circles, triangles, squares, and plus signs are the experimental data for Dy, Nd, Gd, and Sm, respectively. The solid and dotted lines are the TRS calculations for Dy and Nd respectively in (a), and for Gd and Sm in (b).

$\hbar\omega\approx 0.5$ MeV (for each of the two minima), but were kept fixed at all frequencies. The $\nu i_{13/2}$ quasineutron state is out of scale at low frequency in Fig. 7(a) and crosses with the lowest $N=4$ positive parity state at $\hbar\omega\approx 0.7$ MeV, while in Fig. 7(c) it is the lowest positive parity configuration above $\hbar\omega\approx 0.15$ MeV. It should be noted that the calculations corresponding to the $\nu i_{13/2}$ minimum for ^{143}Dy and ^{137}Nd quasineutrons are very similar, since they are isotones, and the equilibrium deformations are nearly the same.

Figure 8 presents relative spin plots with respect to a linear reference ($I_{\mathrm{ref}}=0.06\hbar\omega-6.5$) which is a rough description of the ^{143}Dy data [Fig. 8(a)]. The relative spin for ^{137}Nd is about 5 units larger, with a little larger dynamic moment of inertia (the slight upward slope observed). The TRS calculations are also shown in the figure and are in very good qualitative agreement with the experimental results for both nuclei. The moment of inertia for Nd is larger than for Dy, although this effect is overestimated in the calculation. The spin for these two shapes at the same frequency is both calculated and observed to be smaller in the heaviest isotone. In addition, the Dy band is observed down to $I=13/2$, while in Nd, $I=19/2$ was the lowest spin populated. The calculations predict that the shape is stable (at the referred minimum) in Dy in the frequency range from 300 keV to 500 keV, coinciding very well with the range of the band observed experimentally. In Nd the shape is calculated to be stable above 400 keV, roughly coinciding with the beginning of the observed band at about 330 keV. The steep jumps in the theoretical plots correspond to sudden changes in the yrast equilibrium deformation. For the other two intermediate isotones (^{139}Sm, ^{141}Gd) there is reasonably good agreement [Fig. 8(b)], and there appears to be a strong suggestion of a transition between the two deformation minima as predicted by TRS calculations. However, the amount of the alignment increase in the transition is overestimated. In summary, there is a good overall interpretation for the positive parity bands of the $N=77$ isotones assuming competition between the two positive parity minima with the two distinct configurations. The general trends are predicted by the TRS calculations.

In the alternative assignment of the $i_{13/2}$ basic configuration (and shape) for all of these bands, the behavior of the relative spins (as in Fig. 8) could perhaps be explained by the possibility that a pair of $h_{11/2}$ quasiprotons align generating the observed upward slopes in Sm and Gd. The crossing frequency would be increasing from $Z=60$ to $Z=66$, as expected, since the proton chemical potential is being raised. In this case the Dy band would be completely below the crossing while that of Nd would be completely above. The 5 units of spin difference would come from the alignment of the quasiproton pair. Although this is a satisfactory interpretation, the predicted crossing frequencies of the $h_{11/2}$ proton pair (from calculations of the same type as in Fig. 6) have only a modest increase from 0.28 MeV to 0.38 MeV from Nd to Dy. In Gd the quasiproton alignment has been considered ''perturbed.'' It appears to be delayed and to have an unusually large interaction strength. The situation is, therefore, also not very clear.

In ^{137}Nd the measured transition quadrupole moment is consistent with the predicted $\beta\approx 0.3$ deformation, when the positive γ deformation (towards the noncollective shape) is taken into account [26]. For ^{143}Dy, a similar transition quadrupole moment is expected, since the negative γ (in the collective sector) compensates for the decrease in β deformation.

V. CONCLUSIONS

The high spin states of the very neutron deficient nucleus of ^{143}Dy have been measured for the first time. Among the structures observed, there is a $M1$ band, somewhat irregular, and a very regular positive parity band presenting large dynamic moment of inertia. Two possible assignments have been considered for the configuration of this band, with different deformations: one based on the $i_{13/2}$ coupled to $N_{\mathrm{osc}}=5$ quasineutron states, and the other on low-j $N_{\mathrm{osc}}=4$ positive parity states coupled to high-j $N_{\mathrm{osc}}=5$ protons and neutrons. We suggest that this second configuration could also be involved in the perturbed positive parity bands of the Gd and Sm isotones. It would be interesting to measure lifetimes of the individual states of these bands. In order to distinguish between the two possible assignments, a g-factor measurement would be adequate, since they differ, among other things, by a broken pair of protons. This is a very difficult measurement, however, due to the weak relative intensity of the gamma cascade and the short lifetimes expected.

ACKNOWLEDGMENTS

We thank G. Manente for the preparation of the targets, and the staff of the XTU-Tandem of LNL for the smooth operation of the accelerator. This work was partially supported by the Fundação de Amparo à Pesquisa do Estado de São Paulo (FAPESP) and the Conselho Nacional de Desenvolvimento Científico e Tecnológico (CNPq), Brazil.

[1] G. Andersson, S. E. Larsson, G. Leander, P. Möller, S. G. Nilsson, I. Ragnarsson, S. Åberg, R. Bengtsson, J. Dudek, B. Nerlo-Pomorska, K. Pomorski, and Z. Szymański, Nucl. Phys. **A268**, 205 (1976).
[2] E. S. Paul *et al.*, Phys. Rev. Lett. **61**, 42 (1990) and references therein.
[3] R. Ma *et al.*, J. Phys. G **16**, 1233 (1990).
[4] E. S. Paul *et al.*, J. Phys. G **18**, 121 (1992).
[5] P. H. Regan *et al.*, J. Phys. G **18**, 847 (1992).
[6] P. Willsau *et al.*, Phys. Rev. C **48**, R494 (1993).
[7] D. Bazzacco *et al.*, Phys. Lett. B **309**, 235 (1993); Phys. Rev. C **49**, R2281 (1994).
[8] C. M. Petrache *et al.*, Nucl. Phys. **A617**, 228 (1997).
[9] C. Rossi Alvarez *et al.*, Phys. Rev. C **54**, 57 (1996).
[10] S. M. Mullins *et al.*, Phys. Rev. C **47**, R2447 (1993).
[11] N. H. Medina, F. Brandolini, D. Bazzacco, P. Pavan, C. Rossi-Alvarez, R. Burch, S. Lunardi, R. Menegazzo, M. De Poli, G. Maron, R.V. Ribas, and M. Ionescu-Bujor, Nucl. Phys. **A589**, 106 (1995).
[12] R. Wyss, J. Nyberg, A. Johnson, R. Bengtsson, and W. Nazarewicz, Phys. Lett. B **215**, 211 (1988).
[13] Jing-ye Zhang and N. Xu, Phys. Rev. C **43**, 2449 (1999).
[14] F. R. Espinoza-Quiñones *et al.*, Phys. Rev. C **60**, 054304 (1999).
[15] D. Bazzacco, in Proceedings of the International Conference on Nuclear Structure at High Angular Momentum, Ottawa, 1992, Report No. AECL 10613, Vol. 2, p. 376.
[16] E. Farnea *et al.*, Nucl. Instrum. Methods Phys. Res. A **400**, 87 (1998).
[17] P. Spolaore, J. D. Larson, C. Signorini, S. Beghini, Z. Xi-Kai, and S. Hou-Zhi, Nucl. Instrum. Methods Phys. Res. A **238**, 381 (1985).
[18] P. Spolaore *et al.*, Nucl. Instrum. Methods Phys. Res. A **359**, 500 (1995).
[19] F. Pühlhofer, Nucl. Phys. **A280**, 267 (1977).
[20] W. T. Milner, Holifield Heavy Ion Research Facility Computer Handbook, Oak Ridge National Laboratory, Oak Ridge, Tennessee, 1987.
[21] D. Radford, Nucl. Instrum. Methods Phys. Res. A **361**, 297 (1995).
[22] F. Iachello and D. Vretenar, Phys. Rev. C **43**, 945 (1991).
[23] S. Frauendorf, Z. Phys. A **358**, 163 (1997).
[24] F. Brandolini *et al.*, Phys. Lett. B **388**, 468 (1996).
[25] F. G. Kondev *et al.*, Phys. Rev. C **60**, 011303 (1999).
[26] C. M. Petrache *et al.*, Phys. Lett. B **383**, 145 (1996).